# Holographic Testing of Terahertz Antennas

Gary Junkin, Tao Huang, and John C. Bennett

***Abstract*—In the light of future applications involving Terahertz antenna measurements, this paper revisits Gabor holography as a direct method for recovering phase, offering some interesting advantages for near-field measurements. In particular, we examine the theory and parameterization of planar near-field Gabor holography and comment on the requirements for scanner precision at Terahertz frequencies.**

***Index Terms*—Antenna measurements, antenna radiation pattern, Gabor holography, holographic interferometry, Terahertz, Terahertz radiation.**

## I. Introduction

HOLOGRAPHY was invented in 1947 by Gabor [1] while working to improve the resolution of an electron microscope. The holographic technique using an off-axis reference beam for separation of the real and conjugate image was developed by Leith and Upatnieks as an extension to the Gabor technique (and is often referred to as Leith–Upatnieks holography). A brief history of the development of these techniques is given in Goodman [2]. In 1968, in the Soviet Union [3] probably the first microwave hologram of a reflector antenna was performed and then later, independently in 1974 in the U.K. by Bennett [4] and Anderson [5], initially using coherent optical techniques to recover the antenna aperture function. Although the advent of the fast Fourier transform (FFT) algorithm and digital computers consequently led to much better quality reconstructions, Gabor holographic antenna measurements were to be superseded by direct measurement of phase using two-channel locked receivers and consequently ceased to be of any real practical significance. The term *microwave holography* has, in the context of antennas, evolved to mean phase and amplitude measurements; with a cable reference in the case of near-field measurements or with a free-space wave reference and separate reference antenna in the metrology of deep-space network antennas. The classical Gabor holographic principle strictly speaking is somewhat different since only intensity measurements are made, but the fact that in both cases all the information is recorded justifies the continued use of the term holography. In this paper, we distinguish between *phase and amplitude* measurements involving a two channel receiver and *Gabor holography* involving intensity measurements only.

There are several difficulties with established near-field techniques when contemplating Terahertz measurements. The first arises from the huge number of wavelengths in the path between transmitter and receiver, an order of two greater than in typical microwave measurements. Maintaining a stable reference channel not only requires a very stable source, but also an improvement in mechanical and temperature stability by a factor of 100 compared to current practice at microwave frequencies. Moreover, atmospheric effects are also significant at these frequencies [6] and signal-path fluctuations suggest that a special anechoic environment may be needed. There is also the mechanical tolerance on the scanning surface, again a factor of 100 more stringent than at microwave frequencies. Aside from these, large Terahertz antennas present a further difficulty common to all near-field methods—that of rapid acquisition of huge quantities of phase and amplitude data. Because a typical near-field signal budget requires sensitivity down to $-120$ dBm, receiver bandwidth is limited to about 10 kHz and, hence, signals are downconverted using the superheterodyne principle. An interesting observation is that conventional vector receivers will suffer significantly from Doppler frequency shift effects when scanning Terahertz antennas at speeds of 0.033 m/s (2 m in 60 s). In principle, it may be possible to record intensity data faster than amplitude and phase data, particularly if digital sampling of the final intermediate frequency is carried out at a relative high rate.

There are two candidate methods that utilize intensity measurements and thus avoid most of the problems associated with the measurement of phase in the near-field. Gabor holography records the interference intensity pattern formed between the antenna under test (AUT) and a transmitted reference wave. Alternatively, the more recent technique of phase retrieval utilizes numerical algorithms to iteratively recover phase information from two planes of scanned intensity data. Although phase-retrieval algorithms have been devised to operate effectively under some circumstances [7], the accuracy of the final solution is always unknown since the near-field error metrics available from any fit to intensity data are not directly related to the accuracy of the phase solution. Phase-retrieval accuracy is, in fact, dependent on scan geometry and the antenna under test. The phase-retrieval problem becomes increasingly difficult at Terahertz frequencies for large antennas since at scan distances less than $0.01D^2/\lambda$ there is insufficient phase-retrieval convergence for accurate far-field prediction [8].

One of the earlier obstacles with Gabor holography was the limited dynamic range due to quantization errors that occurred with earlier methods of digitization using power detectors. Using modern heterodyne instrumentation with digital sampling, it is now possible to achieve both high dynamic range and high sensitivity. Volume of data and, hence, scan-time is clearly still an issue in near-field Terahertz measurements and in particular with holograms. Some recent and interesting work using infrared cameras as two-dimensional (2-D) intensity detectors and high power transmitters [9] potentially resolves the scan-time dilemma but has poor dynamic range and impracticably high power levels for Terahertz applications.

Manuscript received January 22, 1999; revised November 29, 1999.

The authors are with the Department of Electronic and Electrical Engineering, University of Sheffield, Sheffield S1 3JD U.K.

Publisher Item Identifier S 0018-926X(00)02463-7.

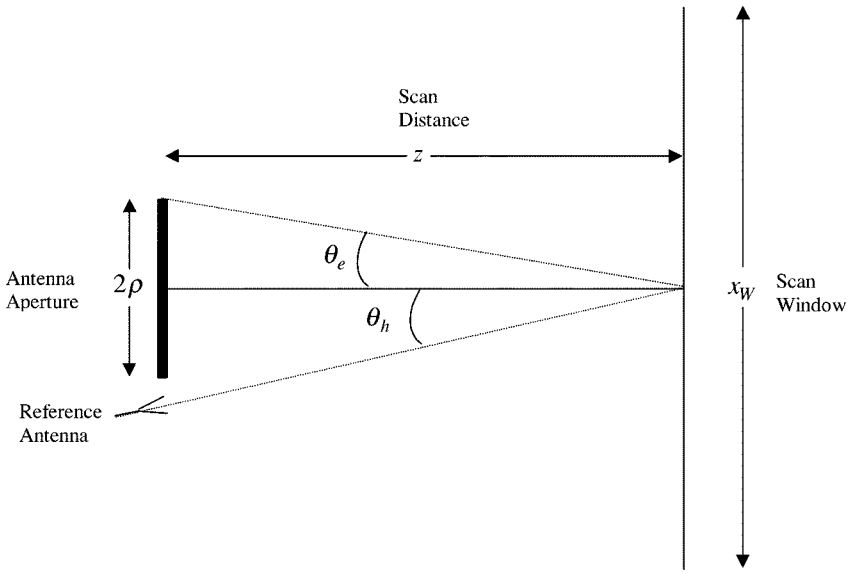


Fig. 1. Schematic diagram of hologram geometry.

As we demonstrate later in this paper, optimum hologram performance is achieved by linear recording of field magnitude, not intensity. Given the previous sensitivity requirements in near-field measurements, scanning techniques with standard receivers are certain to be extremely time consuming at Terahertz frequencies. However, it is very unlikely that conventional coverage of the entire far field will be required or even possible. First, large Terahertz antennas will have extremely directive patterns and any significant extraneous sidelobe structure, such as spillover from subreflectors, is also likely to be very directive. Second, the mechanical tolerance requirement on a planar near-field scanner for close-in measurements (less than an antenna radius) is extremely high (better than $\lambda/100$) for even modest far-field dynamic range (60 dB) predictions. With antenna gains of 80 dB, much of the far-out antenna sidelobe stucture will be obscured by random variations.

In this paper, we determine the relationships governing truncation in $K$-space of near-field Gabor holograms and, hence, derive the requirements for planar sampling. A numerical simulation model is developed and used to investigate the performance of Gabor near-field holography in terms of scanner precision, receiver drift and noise floor. Final simulations are presented to demonstrate the feasibility of the method for large Terahertz antennas using a spherical reference wave and moving further back from the antenna (five to ten diameters) to limit prediction angle coverage, relax sampling interval requirements, and reduce sensitivity to $x$–$y$ positional errors.

## II. Planar Near-Field Hologram Theory

The basis of holography is to create an interference pattern between the AUT and a secondary small reference antenna. The secondary antenna beam must be well defined so that it can be removed numerically in the subsequent reconstruction process. The intensity of the resultant interference pattern $H(\boldsymbol{r})$, created by the reference wave $R(\boldsymbol{r})$ and the AUT beam $S(\boldsymbol{r})$, is recorded at the scan plane either directly using a square law detector (not preferred) or indirectly by recording field magnitude and squaring numerically

$$H(\boldsymbol{r}) = |S(\boldsymbol{r}) + R(\boldsymbol{r})|^2 \tag{1}$$

$$H(\boldsymbol{r}) = S(\boldsymbol{r})S^*(\boldsymbol{r}) + R(\boldsymbol{r})R^*(\boldsymbol{r}) + S(\boldsymbol{r})R^*(\boldsymbol{r}) + R(\boldsymbol{r})S^*(\boldsymbol{r}). \tag{2}$$

Two methods have been used to recover the phase information encoded in the hologram of (2). Historically, the traditional *total hologram* method [10], involves spatial filtering of a complete single hologram of the form in (2), separating undesirable terms, followed by removal of the complex reference field. An improved method [11] utilizes *two* modified holograms, where the first two terms of (2) are removed numerically and the second hologram requires the reference phase to be modified by a fixed known phase angle. Patterns of the AUT magnitude as well as the reference magnitude and phase are therefore required. In the latter reconstruction method, no spatial filtering takes place and consequently there is practically no limitation in operating frequency and there are no special requirements on the position of the reference antenna or on the scan distance. In the former case, the system is less complex and less data are required, but special attention must be applied to sampling and reference horn position.

In this paper, both the reference and AUT field intensities are removed, creating a single modified hologram $H_m(\boldsymbol{r})$

$$H_m(\boldsymbol{r}) = H(\boldsymbol{r}) - S(\boldsymbol{r})S^*(\boldsymbol{r}) - R(\boldsymbol{r})R^*(\boldsymbol{r}). \tag{3}$$

It is anticipated that such a scheme would work well provided receiver drift for all three measurements (AUT, reference, and hologram) were controlled, i.e., these three measurements should occur simultaneously in a specially designed hologram receiver switching subsystem. $H_m(\boldsymbol{r})$ is subsequently Fourier transformed to $K$-space to separate out cross-correlation terms, resulting in

$$H_m(\boldsymbol{k}) = S(\boldsymbol{k}) \otimes R^*(-\boldsymbol{k}) + R(\boldsymbol{k}) \otimes S^*(-\boldsymbol{k}). \tag{4}$$

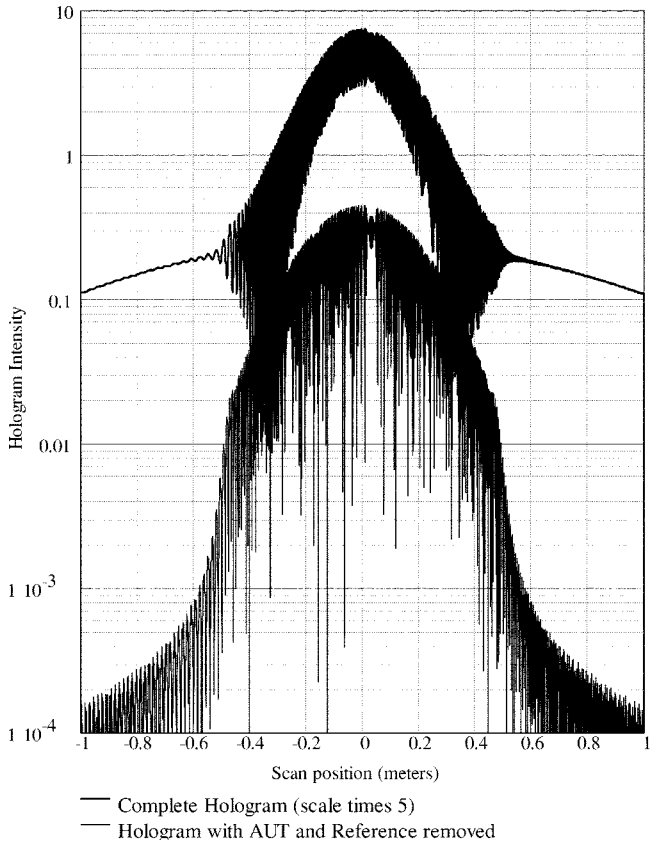


Fig. 2. Modified and unmodified holograms simulated for a 1-m aperture at 1 THz. The scanner is ideal, SNR is 73 dB, data recording 16 bit linear, and drift is set to 0.1%.

The method relies on being able to spatially separate one of the terms in (4). A choice of reference wave is therefore necessary and we now consider the following two cases; plane wave and spherical wave reference.

### A. Case I: Plane Wave Reference

A simple interpretation of (3) arises if $R(\boldsymbol{r})$ is an ideal plane wave of the form

$$R(\boldsymbol{r}) = A_R \exp(j\boldsymbol{k}_r \cdot \boldsymbol{r}) \operatorname{rect}\left(\frac{x}{x_W}\right) \operatorname{rect}\left(\frac{y}{y_W}\right) \tag{5}$$

where $\boldsymbol{k}_r$ is a propagation vector describing the direction of the reference plane wave and $x_W$, $y_W$ are the scan dimensions.

The cross-correlation between AUT and reference waves $S(\boldsymbol{k}) \otimes R^*(-\boldsymbol{k})$, commonly referred to as the image term and denoted here as $I_{\otimes}(\boldsymbol{k})$, is particularly straightforward for the plane wave case

$$\begin{aligned} I_{\otimes}(\boldsymbol{k}) &= S(\boldsymbol{k}) \otimes R^*(-\boldsymbol{k}) \\ &= \int_{-\infty}^{+\infty} S(\boldsymbol{k'}) A_R^* \operatorname{sinc}[x_W(k'_x - k_x + k_{xr})] \\ &\quad \cdot \operatorname{sinc}[y_W(k'_y - k_y + k_{yr})]\, d\boldsymbol{k'} \\ &\xrightarrow{x_W,\, y_W = \infty} A_R^* S(\boldsymbol{k} + \boldsymbol{k}_r). \end{aligned} \tag{6}$$

In the limit, as the scan window tends to infinity, the *image* term $I_{\otimes}(\boldsymbol{k})$ is a replica of the AUT plane wave spectrum weighted by the conjugate of the reference wave transform amplitude $A_R^*$ and shifted in $K$-space to $-\boldsymbol{k}_r$. The conjugate *image* term

$$I_{\otimes}^*(\boldsymbol{k}) = R(\boldsymbol{k}) \otimes S^*(-\boldsymbol{k}) = A_R S^*(\boldsymbol{k} - \boldsymbol{k}_r) \tag{7}$$

is again a weighted replica of the AUT plane wave conjugate spectrum, reflected and shifted in $K$-space to $+\boldsymbol{k}_r$.

### B. Case II: Spherical Wave Reference

A spherical off-axis wave from a source at $(x_R, y_R, z)$ gives rise to a cross-correlation integral that truncates as shown in the Appendix $(y_R = 0)$ when

$$\left| z \frac{k}{k_o} - x_R \right| > \rho. \tag{8}$$

This leads to a maximum $x$-directed spatial frequency component of

$$k_x^{\mathrm{MAX}} = \frac{(\rho + x_R)k_o}{z} \tag{9}$$

and a corresponding maximum $y$-directed spatial frequency component of

$$k_y^{\mathrm{MAX}} = \frac{(\rho + y_R)k_o}{z}. \tag{10}$$

The *image* term (shown later in Fig. 3) results from a spatially extended but truncated, aperture-like function of approximate width $2\theta_e$, which is approximately centered in $K$-space at $\theta_h$ where $\theta_e$, $\theta_h$ are defined in Fig. 1.

The spherical reference wave is fundamentally advantageous for three reasons. First, the scan-plane edge illumination can be controlled and so correspondingly lowers the reference on-axis sidelobes. Second, the image terms no longer have the form of the AUT plane-wave spectrum, so dynamic range in $K$-space is substantially reduced. Third, the image term is band-limited in $K$-space, resulting in the sampling interval requirements given in (9) and (10) as opposed to normal sampling requirements [12].

## III. Data Registration (Grid) Error Analysis

Because planar near-field analysis relies heavily on the convolution theorem in rectangular coordinates, there is an implicit assumption that the surface over which the data are recorded is perfectly flat. Furthermore, as the FFT is used to evaluate the spectra, there is also an implicit assumption that the data are registered on a perfectly sampled rectangular grid. A comprehensive treatment planar near-field error analysis is given in [13]. Here we briefly address the issue of registration errors in the context of Gabor holography.

The modified hologram recorded on a nonperfect grid described by $\boldsymbol{r'}$is

$$H_m(\boldsymbol{r'}) = S(\boldsymbol{r'})R^*(\boldsymbol{r'}) + R(\boldsymbol{r'})S^*(\boldsymbol{r'}) \tag{11}$$

where $\boldsymbol{r'} = \boldsymbol{r} + \Delta\boldsymbol{r}$ and $\Delta\boldsymbol{r} = (\Delta x, \Delta y, \Delta z)$ describes the set of registration errors associated with the probe position. We

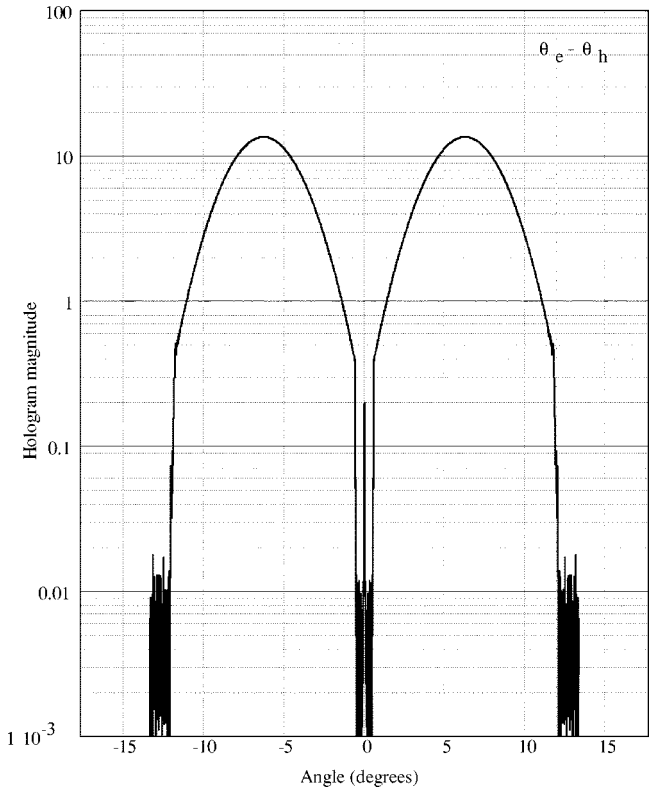


Fig. 3. Fourier transform of the modified hologram shown in Fig. 2, showing image and conjugate image with residual background level at 0.1% of peak image value.

now investigate the effect of registration errors on the cross-correlation functions. The following mathematical outline is useful also in programming a full simulation model for 2-D data sets since it relates perfect-grid data to nonperfect-grid data through the use of the Fourier transform.

For any complex distribution $A(r)$, the truncated Taylor series expansion leads to the following approximation for $A(r+\Delta r)$

$$A(r+\Delta r) \approx A(r) + \frac{\partial}{\partial x}[A(r)]\Delta x + \frac{\partial}{\partial y}[A(r)]\Delta y + \frac{\partial}{\partial z}[A(r)]\Delta z. \quad (12)$$

The partial derivative of the complex field distribution is conveniently determined through use of the Fourier transform. The complex field gradients are given by

$$\frac{\partial}{\partial p}[A(r)] = \Im^{-1}[jk_p A(k)] \qquad p \to x, y, z \quad (13)$$

where $k_z = \sqrt{k_o^2 - k_x^2 - k_y^2}$ and $A(k) = \Im[A(r)]$ denotes the Fourier transform. Turning our attention to intensity functions, we can now develop the distorted $K$-space image term due to registration errors. First consider $x$-directed errors and then general expressions. By expanding terms in the intensity function and ignoring second-order products in the components of $\Delta r = (\Delta x, \Delta y, \Delta z)$, then

$$\begin{aligned} I_{\otimes}(r') &\approx S(r)R^*(r) + S(r)\frac{\partial}{\partial x}[R^*(r)]\Delta x \\ &\quad + S^*(r)\frac{\partial}{\partial x}[R(r)]\Delta x \\ &\approx S(r)R^*(r) + 2\Delta x \,\mathrm{Re}\left[S(r)\frac{\partial}{\partial x}[R^*(r)]\right]. \end{aligned} \quad (14)$$

The effect of errors are obtained in $K$-space by Fourier transforming the above, leading to

$$\begin{aligned} I'_{\otimes}(k) &\approx I_{\otimes}(k) + S(k) \otimes [jk_x R^*(-k)]\Delta x + S^*(-k) \\ &\quad \otimes [jk_x R(k)]\Delta x. \end{aligned} \quad (15)$$

The effect of grid errors is to create additional contributions that emerge from convolutions involving $jk_x R(k)$. For errors in $y$ and $z$, there will be similar convolution terms involving $jk_y R(k)$ and $jk_z R(k)$, respectively. Hence, the choice of reference wave influences the effect of scanner registration errors. Since $k_z$ is approximately constant for small angles and tends to zero for $k_x^2 + k_y^2 = k_o^2$, we expect errors in $z$ to have a quite different effect on the $K$-space cross-correlation functions than errors in $x$ or $y$. This is indeed the case. The hologram cross-correlation functions, while insensitive to $z$-errors, tend to spread out in the presence of scan registration errors in $x$ or $y$, particularly if these errors are random in nature. Furthermore, as expected, increasing the reference off-axis angle results in increased sensitivity to scan axis registration errors. For this reason we choose to place the reference horn as close as possible to the antenna, ideally near the rim of the reflector. Numerical simulations are presented in Section VI to illustrate data registration errors and a comparison is made with complex (phase and amplitude) measurements.

## IV. Quantization Errors

Early attempts at recording holograms were based on square law detectors that not only have poor sensitivity but also suffer greater quantization errors from the fact that they measure power. At Terahertz frequencies the current technologies for power and field strength measurements are discussed in [6]. The disadvantage for weak signals of directly digitizing the power distribution lies with the poor use of available quantization levels. Consider a field distribution $E$, which has been amplified to have a peak magnitude of unity. A quantization error of $\delta n$ in the measurement of $|E|$ manifests itself as an absolute error in the computed value of $|E|^2$ of $2\delta n|E|$, whereas the same quantization error in the direct measurement of $|E|^2$ manifests itself as an absolute error in $|E|^2$ of $\delta n$. When $|E| < 0.5$, it is therefore advantageous to digitize $|E|$ first and subsequently square numerically. The values of $\delta n$ depend upon the number of bits available and whether linear or logarithmic recording is used. Simulations with a

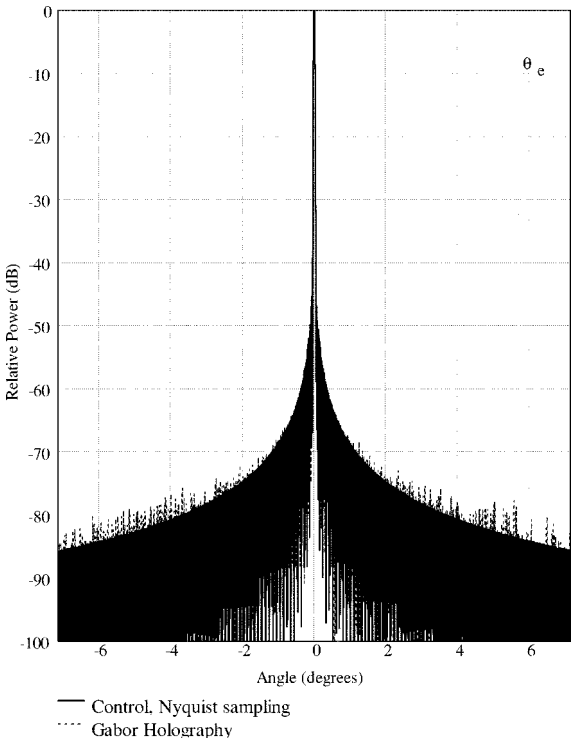


(a)

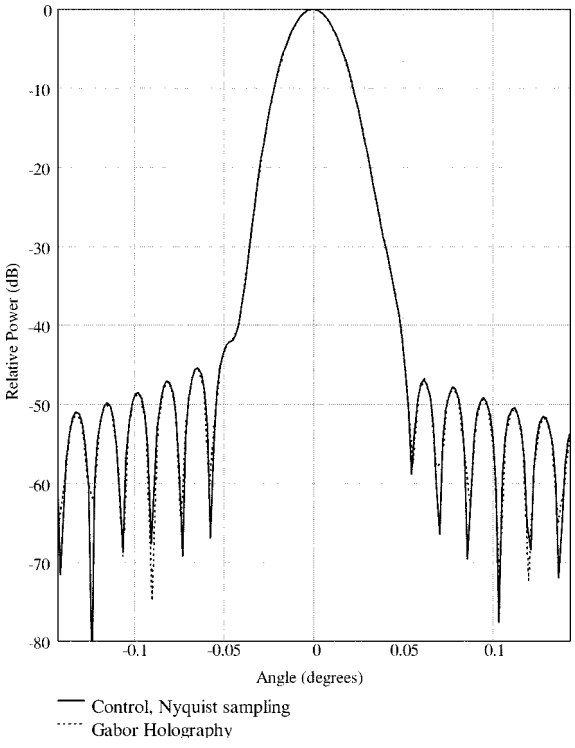


(b)

Fig. 4. Predicted far-field for the 1 THz ideal scanner simulation of Fig. 2. Prediction is valid within the angle set by $\theta_e$. (a) Full angular range. (b) Reduced angular range showing detail near main beam.

−30 dB edge taper Gaussian beam [10] have shown that linear recording is far superior to logarithmic and that 16 bits are sufficient to reduce far-field quantization induced errors to levels better than −100 dB with respect to mainbeam. In our simulation, the sampling operation $D(V)$ operating on voltage $V$ (in the range 0–1) is modeled as

$$D(V) = \frac{INT(2^b V + RAN)}{2^b} \tag{16}$$

where

| | |
|---|---|
| $b$ | number of bits in the analog to digital converter; |
| $RAN$ | random number between zero and one; |
| $INT()$ | takes the integer part of a real number. |

## V. $K$-Space Filtered Holographic Reconstruction Process

The $K$-space modified hologram reconstruction process relies upon the spatial separation of the two image terms of $H_m(\boldsymbol{k})$ in $K$-space. The interference pattern $H_m(\boldsymbol{r})$ is Fourier transformed and $H_m(\boldsymbol{k})$ is subsequently spatially filtered to extract either $I_{\otimes}(\boldsymbol{k})$ or $I^*_{\otimes}(\boldsymbol{k})$. Further inverse transformation yields $S(\boldsymbol{r})\cdot R^*(\boldsymbol{r})$ or $R(\boldsymbol{r})\cdot S^*(\boldsymbol{r})$ so precise knowledge of $R(\boldsymbol{r})$ is required to accurately determine $S(\boldsymbol{r})$. While we can easily measure the magnitude of the reference wave $|R(\boldsymbol{r})|$, the reference wave phase $\arg(R(\boldsymbol{r})$ (requires greater attention. In this paper, we propose that $\arg(R(\boldsymbol{r}))$ is calculated based on the premise that the reference source is a well defined antenna of 20–30 dB gain that produces a spherical wavefront or one that can be specified. We believe this is an engineeringly feasible solution, although it may place additional demand on the performance of scan axis accuracy, as discussed later in this paper. In common with the idea of the quiet zone quality of a CATR, verification of the quality of the reference wavefront is necessary in order ultimately to determine prediction accuracy. It may be possible to experimentally validate the reference wave by analyzing a hologram created with a small antenna identical to the reference horn, using the hologram reconstruction method of [10], but so far this has not been attempted.

## VI. Numerical Simulations

Simulations have been carried out at 100 GHz and 1 THz for a 1-m diameter scalar aperture model. The choice of 1-m diameter parallels the study in [6]. It is assumed that the power source delivers 10 dBm. For a Gaussian aperture illumination of 30-dB edge taper, this results in a peak power density of 19.4 dBm/m$^2$, which is approximately invariant along the $z$-axis for scan distances less than about $0.005D^2/\lambda$ (16 m). The probe antenna has a gain of 20 dB and an effective area of −61.4 dBm$^2$ resulting in a peak signal from the AUT of approximately −42 dBm into a Terahertz receiver. The reference peak signal is arranged to be 13 dB less than the peak AUT signal. Assuming a receiver bandwidth of 10 kHz and a noise temperature of 20 000K (SSB), the peak signal-to-noise ratio is, therefore, approximately 73 dB. A schematic of the hologram setup is shown in Fig. 1, where a standard measurement distance of 5 m is used. The required reference horn gain is then approximately 20 dB plus the positive value of the waveguide coupling

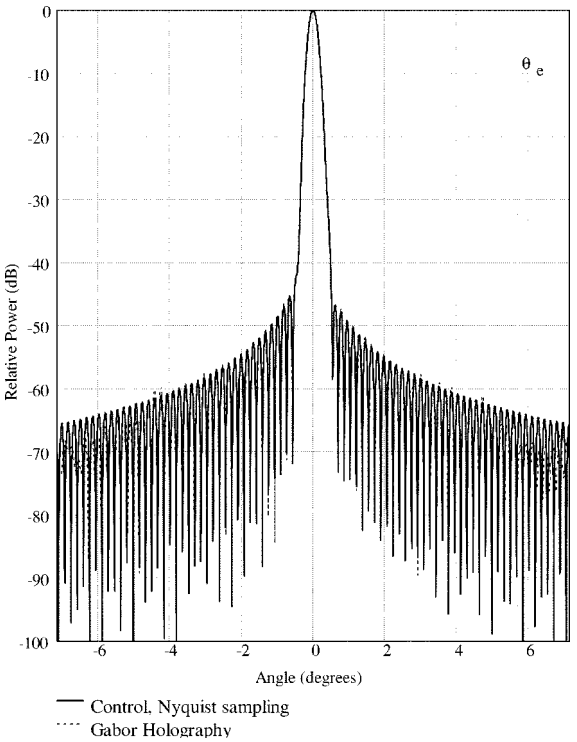


(a)

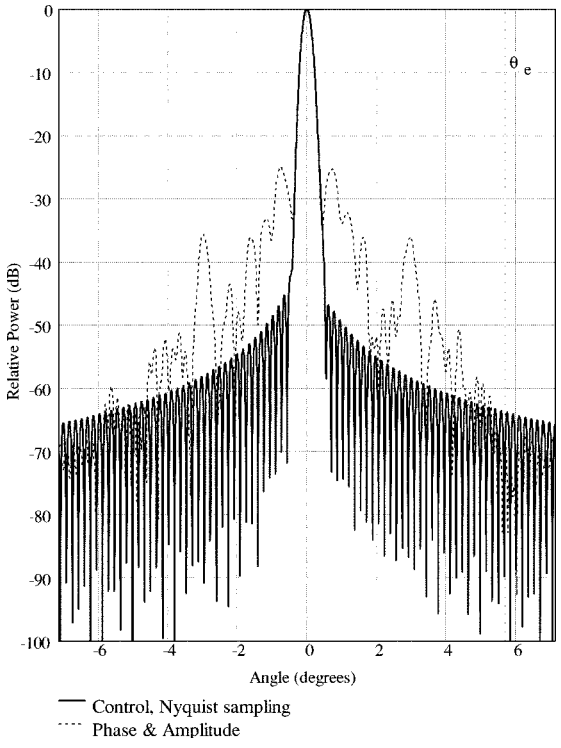


(b)

Fig. 5. Effect of planarity ($z$-axis) errors simulated at 100 GHz for $\lambda/20$ random variations. (a) Gabor holography prediction. (b) Complex (phase and amplitude) prediction.

loss. Throughout the simulations, the number of bits is 16. Both 1-D and 2-D simulation models have been developed, but for brevity we restrict our attention here to the 1-D model.

The 1-D simulation model is useful for testing Terahertz holograms at full sampling ($\lambda/2$) and is based on a Huygens' principle summation over an aperture function with Gaussian amplitude taper (of 30 dB) and phase errors consisting of quadratic, cubic, and sinusoidal (arranged to produce strong sidelobes for testing aliasing effects). The 1-D simulated aperture function is sampled at half-wavelength intervals and has the form

$$S(x) = \exp\left(-\frac{x^2}{\sigma^2} + jk_o\left[a\lambda\left(\frac{x}{\rho}\right)^2 + b\lambda\left(\frac{x}{\rho}\right)^3 + c\lambda\sin\left(n\pi\frac{x}{\rho}\right)\right]\right) \cdot \text{rect}\left(\frac{x}{2\rho}\right) \tag{17}$$

where

- $\sigma$ chosen to give 30-dB edge taper;
- $\rho$ half the aperture width;
- $a$ has the value 0.04;
- $b$ has the value 0.06;
- $c$ has the value 0.004;
- $n$ controls the spurious sidelobe position.

The value of $n$ has been chosen to give sidelobes representative of spillover at 20°. The 1-D simulation model includes random $y$ and $z$ errors and random digitization errors as well as receiver noise at 73 dB SNR. A control far-field is setup by half-wavelength integration of the aperture function at a close scan distance of 0.5 m and subsequently applying a Fourier transform. The Gabor holograms are created by integrating the aperture over the scan plane at sampling intervals given by

$$\delta = \frac{\pi}{f_K k_o(\tan\theta_e + \tan\theta_h)} \tag{18}$$

where $f_K = 1.1$ ensures an additional 10% margin in $K$-space. The angles $\theta_e$, $\theta_h$ are subtended from the scan origin to the edge of the aperture and reference horn position, respectively. The scan distance and aperture size are fixed at 5 and 1 m, respectively. The reference horn position is located at a distance from the aperture edge given by 10% of the aperture radius.

Fig. 2 shows the modified and unmodified holograms recorded at 100 GHz with perfect registration and including receiver noise at 73-dB SNR and 16-bit digitization. Fourier transformation of the modified hologram gives the *image* terms, which are clearly separated in $K$-space, as shown in Fig. 3. Residual background is at a level of approximately 0.1% of the peak *image* value, resulting in extremely good reproduction of the far-field within the prediction angle set by $\theta_e$ as shown in Fig. 4(a) and (b).

### A. Planarity Registration Errors

The effect of planarity errors for random variations up to $\lambda/20$ along the $z$-axis are shown in Fig. 5(a) and (b), comparing the

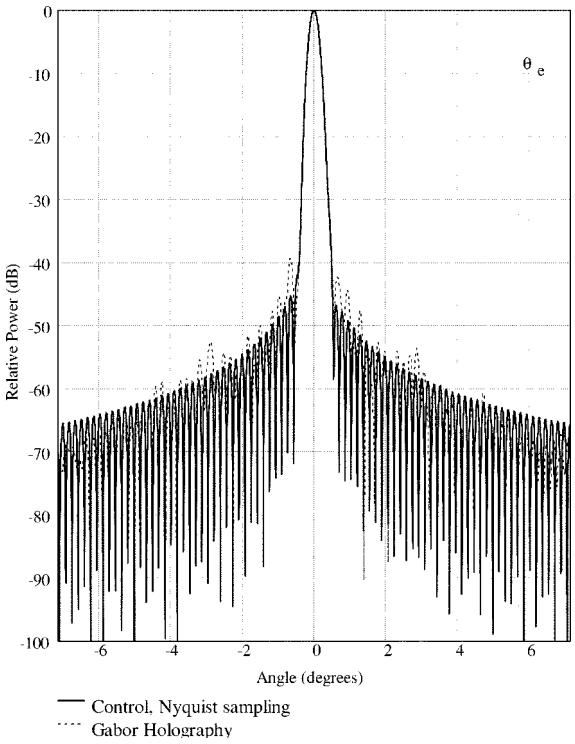


(a)

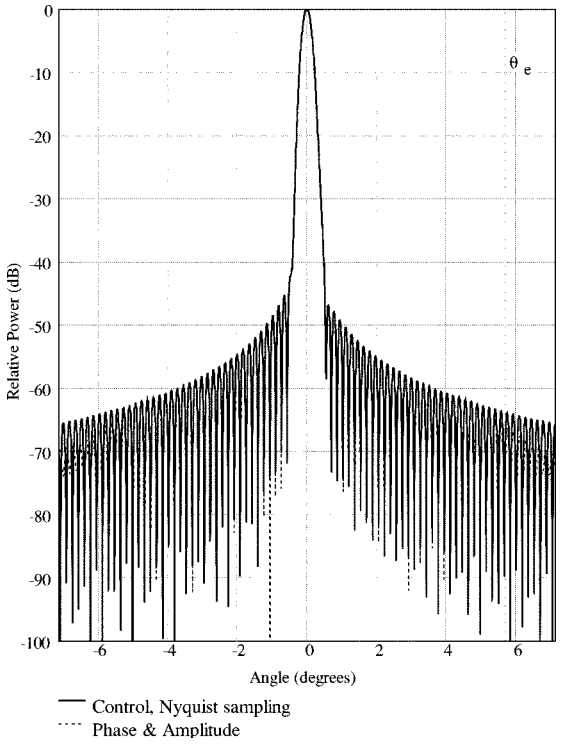


(b)

Fig. 6. Effect of scan-axis errors simulated at 100 GHz for $\lambda/20$ random variations. (a) Gabor holography prediction. (b) Complex (phase and amplitude) prediction.

performance of holography with phase and amplitude measurements. As expected, complex phase and amplitude measurements are extremely sensitive to $z$-axis errors and errors of $\lambda/20$ are completely unacceptable. Also as expected, holography is shown to be immune to this kind of error.

### *B. Scan-Axis Registration Errors*

Scan-axis registration errors, again with random variations of peak value $\lambda/20$, were introduced for an otherwise perfect scan plane. A comparison between holography and phase and amplitude, shown in Fig. 6(a) and (b), indicates poorer performance by holography. The residual $K$-space background has now risen to approximately 1% of the peak image level. The relatively poor performance by holography is due primarily to the fact that the reference wave used in reconstruction is calculated on a perfect grid. If the scan-axis registration errors were known, then the prediction capabilities would improve substantially.

### *C. Receiver Drift Effects*

The effect of receiver drift was modeled by introducing three random factors $d_S$, $d_H$, $d_R$ for the signal, reference, and hologram channels, respectively, as

$$\begin{aligned} d_S &= 1 + (RAN - 0.5)d \\ d_H &= 1 + (RAN - 0.5)d \\ d_R &= 1 + (RAN - 0.5)d \end{aligned} \tag{19}$$

where $RAN$ is a random number generator between zero and one and $d$ is the maximum relative drift. The recorded signal, hologram and reference voltages become

$$\begin{aligned} S' &= D(d_S(S + N_S)) \\ H' &= D(d_H(S + R + N_H)) \\ R' &= D(d_R(R + N_R)) \end{aligned} \tag{20}$$

where $D()$ is the digitization operator and $N_S$, $N_H$, $N_R$ are the noise in the three channels, respectively. The modified hologram used for reconstruction becomes

$$H_m = |H'|^2 - |R'|^2 - |S'|^2. \tag{21}$$

An error of approximately 2 dB at the $-45$-dB sidelobe level occurred in the simulation when $d$ was set to 5%, with a corresponding residual autocorrelation level of 22% *image* peak in $K$-space. Values of drift less than 1% produced insignificant far-field error and consequently the default value of $d$ for all simulations was chosen as 0.1%.

### *D. Receiver Noise Floor And Scan Time*

An approximate rule of thumb for complex field measurements is to allow a maximum smear distance of 10% of the sampling interval. If the receiver bandwidth is 10 kHz and the receiver takes an average of ten samples, then the fastest sampling time is 1 ms, meaning that the scanner can travel

at a maximum speed of $100\delta$ m/s where $\delta$ is the sampling interval in meters. For the 100 GHz simulation $\delta = 2.188\lambda$, giving a maximum scan speed of 0.656 m/s. A scan window of 2 m could then, in principle, be covered in 3 s. For 1 THz, the scan time would increase to 30 s for the same receiver averaging of ten samples.

The worst case Doppler shift in frequency, experienced by the signal channel of a complex receiver, would be $k_o v/2\pi$ Hz, where $k_o$ is the propagation constant and $v$ is the scan velocity in m/s, giving a value of approximately 219 Hz at 1 THz. This is a substantial fraction of the receiver equivalent bandwidth (after averaging), which will upset a standard microwave receiver, leading necessarily to further slowing of the scan speed.

The above argument is based on complex measurements. A further consideration is necessary in order to compare the situation with intensity measurements. We already learned from simulations that holograms are most sensitive to errors in scan axis registration. We have therefore considered smearing effects along the scan axis. A simplified approach has been taken, where the effect of smearing has been approximated by averaging two sets of data displaced by 10% of the sampling interval. The results show that holography is relatively sensitive to smearing effects because of the oscillatory nature of the interference pattern. However, for the hologram geometry tested at 5 m, the effect is significant only for smearing distances greater than 10% sampling interval.

## VII. Conclusions

Gabor holography has some promising features that make it a possible contender for large Terahertz antenna measurements. Modified holograms permit the reference antenna to be positioned close to the AUT, thereby reducing sensitivity to scan axis errors and reducing scan distance. The following bullet points summarize the findings in this paper.

- For Gabor holography to work effectively, typical measurement distances are greater than those applicable to conventional planar near field.
- Measurements and sampling criteria are dependent on geometrical relationships (18).
- Quantization noise with 16-bit linear recording produces insignificant far-field errors.
- There exist additional prediction errors associated with removing the reference wave, since this must be calculated from knowledge of the reference horn pattern and, if scan axis registration errors are unknown, then a tolerance of $\lambda/50$ is advisable.
- Holography is significantly more sensitive to smearing effects during scanning than complex measurements, but the effect is insignificant for the geometry tested, provided a 10% sampling interval criterion is enforced.
- In contrast to complex measurements, holography is very insensitive to planarity errors.
- By utilizing modified holograms, where the reference antenna is located as close as possible to the aperture, the scan distance can be reduced from 15 [11] to 5 m for up to 2-m diameter antennas at 1 THz.
- Relative receiver channel drift at better than 1% levels is sufficient for adequate performance.
- New digital tracking receivers will be needed to fully utilize the advantages of holography and reduce the overall measurement times.

## Appendix A

A spherical off-axis wave from a source at $(x_R, y_R, z_R)$ behaves in $K$-space as

$$R(\boldsymbol{k}) = A_R(\boldsymbol{k}) \exp\left(j\left(z_R\sqrt{k_o^2 - |\boldsymbol{k}|^2} + k_x x_R + k_y y_R\right)\right) \tag{A.1}$$

where $A_R(\boldsymbol{k})$ represent the plane wave spectral components of the reference antenna source. Considering a 1-D AUT with uniformly illuminated rectangular aperture of radius $\rho$ meters, then the image term for a uniform aperture becomes

$$\begin{aligned} I_{\otimes}(k) &= S(k) \otimes R^*(-k) \\ &= \int_{-\infty}^{+\infty} S(k') R^*(k'-k)\, dk' \\ &= \int_{-\infty}^{+\infty} \frac{\sin(\rho k')}{\rho k'} \exp\left(j z_A \sqrt{k_o^2 - k'^2}\right) \\ &\quad \cdot \Big[A_R(k'-k) \exp\Big(j z_R \sqrt{k_o^2 - (k'-k)^2} \\ &\quad + j(k'-k)x_R\Big)\Big]^*\, dk'. \end{aligned} \tag{A.2}$$

By expanding to second order those terms inside square roots, the image term approximately becomes

$$\begin{aligned} I_{\otimes}(k) = \exp\left[j\frac{k^2}{2k_o} z_R - k x_R\right] &\int_{-\infty}^{+\infty} \frac{\sin(\rho k')}{\rho k'} A_R^*(k'-k) \\ &\cdot \exp\left[j(z_R - z_A)\frac{k'^2}{2k_o}\right] \\ &\cdot \exp\left[-j\left(z_R\frac{k}{k_o} - x_R\right)k'\right] dk'. \end{aligned} \tag{A.3}$$

By comparison with the following equation [14]

$$\int_{-\infty}^{+\infty} \frac{\sin(\pi x)}{\pi x} \exp(-j2\pi S x)\, dx = \begin{cases} 1 & |S| < 1/2 \\ 0 & |S| > 1/2. \end{cases} \tag{A.4}$$

If $z_R = z_A = z$ and noting that $A_R(k)$ varies much more slowly than $\sin(\rho k')/\rho k'$, then the integral (A.3) truncates when

$$\left| z\frac{k}{k_o} - x_R \right| > \rho. \tag{A.5}$$

This leads to a maximum $x$-directed spatial frequency component of

$$k_x^{\mathrm{MAX}} = \frac{(\rho + x_R)k_o}{z} = k_o(\tan\,\theta_{ex} + \tan\,\theta_{hx}) \qquad \text{(A.6)}$$

where $\theta_{ex}$ is the angle subtended by the scan origin and the edge of the aperture along $x$ and $\theta_{hx}$ is the angle subtended by the scan origin and the reference $x$ coordinate.

A corresponding maximum $y$-directed spatial frequency component of

$$k_y^{\mathrm{MAX}} = \frac{(\rho + y_R)k_o}{z} = k_o(\tan\,\theta_{ey} + \tan\,\theta_{hy}) \qquad \text{(A.7)}$$

occurs where the corresponding angles now have $y$ subscripts.

In fact, the above sampling criteria relate to the paraxial approximation inherent in truncating the image cross-correlation integral to second order. Numerical evaluation of the full integral reveals that the tangent functions should be replaced with sine functions in the above sampling equations if scan distances of around 1 m are used. For such cases the $K$-space holograms are very oscillatory on one side and the corresponding image boundary is not clearly defined. In any event, the sensitivity to registration errors increases with smaller scan distances and we therefore recommend a choice that permits the paraxial approximation.

## REFERENCES


[1] D. Gabor, "Microscopy by reconstructed wavefronts," in *Proc. Roy. Soc.*, vol. A, London, U.K., 1949, pp. 454–487.

[2] J. W. Goodman, *Introduction to Fourier Optics*. New York: McGraw-Hill, 1968, sec. 8-1.

[3] P. M. Herouni, "Near field microwave holography measurements in USSR," in *Proc. Int. Workshop Holography Testing of Large Radio Telescopes*, Nizhnij Arkhyz, Russia, Sept. 1990, pp. 47–52.

[4] J. C. Bennett, "Investigation of the characteristics of large reflector antennas using microwave holography," Ph.D. dissertation, Univ. Sheffield, U.K., Apr. 1974.

[5] A. P. Anderson, "Microwave holography," in *Proc. Inst. Elect. Eng.*, vol. 124, Nov. 1977, I.E.E. Reviews, pp. 946–962.

[6] P. R. Foster, D. Martin, C. Parini, A. Raisanen, J. Ala-Laurinaho, T. Hirvonen, A. Lehto, T. Sehm, J. Tuovinen, F. Jensen, and K. Pontoppidan, "MMWave antenna testing techniques—Phase 2,", prepared for ESTEC under Contract 11 641/95/NL/PB(SC), Dec. 1996.

[7] G. Junkin, A. P. Anderson, C. A. E. Rizzo, W. J. Hall, C. J. Prior, and C. Parini, "Near-field/far-field phase retrieval measurement of a prototype of the microwave sounding unit antenna Amsu-B At 94 GHz," in *Workshop Millimeter Wave Technol. Applicat.*, Noordwijk, The Netherlands, Dec. 1995, ESA-WPP 098.

[8] G. Trueba and G. Junkin, "Numerical beam alignment procedure for planar near-field phase retrieval," *Electron. Lett.*, vol. 31, no. 14, pp. 1116–1117, July 1995.

[9] C. F. Stubenrauch, K. MacReynolds, J. E. Will, J. D. Norgard, M. Seifert, and R. H. Cormack, "Microwave antenna far-field patterns determined from infrared holograms," in *Proc. 19th Antenna Meas. Tech. Assoc.*, Boston, MA, Nov. 1997, pp. 125–130.

[10] G. Junkin, T. Huang, and J. C. Bennett, "Holographic near-field/far-field for Terahertz antenna testing," in *20th ESTEC Antenna Workshop Millimeter Wave Antenna Technol. Antenna Meas.*. Noordwijk, The Netherlands, June 1997, ESA-W098, pp. 321–328.

[11] C. F. Stubenrauch, K. MacReynolds, A. C. Newell, R. H. Cormack, J. E. Will, and J. E. Norgard, "Phaseless measurements of antenna near fields employing holographic phase retrieval," in *Proc. 18th Antenna Meas. Tech. Assoc.*, Seattle, WA, Sept. 1996, pp. 20–24.

[12] M. H. Francis and T. Milligan, "Aperture sampling effects in planar near-field measurements," in *Proc. 19th Antenna Meas. Tech. Assoc.*, Boston, MA, Nov. 1997, pp. 79–83.

[13] A. C. Newell, "Error analysis for planar near-field measurements," *IEEE Trans. Antennas Propagat.*, vol. 36, pp. 654–668, June 1988.

[14] R. N. Bracewell, *The Fourier Transform and Its Applications*. New York: McGraw-Hill, 1978.



**Gary Junkin** received the B.Eng. degree in electronic engineering, and the Ph.D. degree for work on microwave holography, both from the University of Sheffield, U.K., in 1982 and 1988, respectively.

He was a Research Associate at the University of Sheffield until 1989, when he took a teaching post in the Department of Electronic and Electrical Engineering there. His interests include microwave holography, near-field antenna measurements, and finite-difference time-domain modeling of impulse antennas for ground penetrating radar.

**Tao Huang** received the B.Sc. degree in electronic and electrical engineering from Nanjing University of Aeronautics and Astronautics, China, in 1983, the M.Sc. degree in microwave and antenna engineering from Southeast University, China, in 1988, and the Ph.D. degree from the University of Sheffield, U.K., in 1999.

He is currently a Project Manager/Senior Engineer with CSA Wireless, involving design and development of BTS antennas for group special mobil (GSM) systems and universal mobile telecommunication system (UMTS). His research interests include the development of microwave antennas, antenna near-field and/or far-field measurement techniques and systems, analytical and numerical modeling of electromagnetic radiation and scattering fields, wireless communications, and radar cross section studies of electrically large objects.

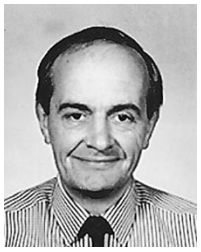

**John C. Bennett** received the B.Eng. and Ph.D. degrees from the University of Sheffield, U.K., in 1970 and 1974, respectively.

Since 1972, he has been a Lecturer, Senior Lecturer, and Reader in the Department of Electronic and Electrical Engineering, University of Sheffield. His primary research interest involves the development of a ground-based synthetic aperture radar system for the study of vegetation communities and environmental parameters. Other research interests include microwave holographic antenna measurements, near-field/far-field transformation techniques, the evaluation of microwave anechoic chambers and far-field ranges, and the free-space measurement of high-loss materials at microwave frequencies.